ACS Energy LETTERS

http://pubs.acs.org/journal/aelccp

Disconnected Lithium Metal Damages Solid-State Electrolytes

Diana Avadanii,* Steffen Ganschow, Markus Stypa, Sonja Müller, Sabrina Lang, Dominik Kramer, Christoph Kirchlechner, and Reiner Mönig*

Cite This: *ACS Energy Lett.* 2025, 10, 2061−2067

Read Online

ACCESS | Metrics & More | Article Recommendations | Supporting Information

ABSTRACT: **Solid-state batteries with a lithium−metal anode are energy-storage devices that promise increased energy density and improved safety compared with liquid systems. Despite significant developments, the chemomechanical degradation of solid-state batteries represents a significant challenge to their widespread adoption. Specifically, Li-filled cracks (called "dendrites") and electronically isolated Li inclusions ("dead" Li) are key defects resulting from coupled electrochemical and mechanical degradation during cycling. In this study, we use a symmetrical Li|LLZO|Li cell with a single-crystal electrolyte and demonstrate that an electronically isolated Li-metal inclusion exhibits bipolarity under an external electrical field, which leads to further crack expansion. We suggest that this process of "dead" metal activation accelerates chemomechanical degradation in solid-state batteries with alkali anodes.**

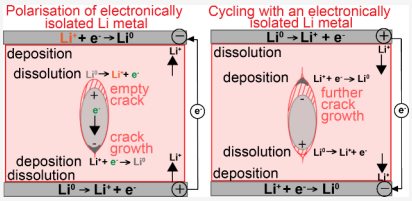

Energy-storage solutions underpin current strategies for the decarbonization of key industries as a step toward achieving carbon neutrality. Using Li-metal anodes (theoretical specific capacity = 3862 mAh g^{-1}) and solid-state electrolytes (e.g., $Li_7La_3Zr_2O_{12}$) improves the energy density and safety of batteries when compared to Li-ion cells using a liquid electrolyte.[1−5] Studies investigating the chemomechanical processes leading to degradation and short circuits in solid-state batteries (SSBs) pinpoint the nucleation and propagation of Li-filled cracks (i.e., "dendrites") as the major challenge in the successful implementation of SSBs.[2−4,6−10]

Li-metal electrodeposition and dissolution can lead to the formation of electronically isolated Li metal (i-Li or "dead" Li) in both liquid Li-ion[11,12] and solid-electrolyte cells.[6,13−16] In liquid Li-ion cells, the formation of electronically disconnected Li is a primary cause of capacity loss and degradation.[11,17] In solid-state cells, these i-Li islands could be generated during reversal of Li plating and stripping,[13,14,18] or during heterogeneous Li plating within the grain-boundary network of the solid-state electrolyte.[19−25] However, the response during cycling and the impact of these isolated Li-metal inclusions on SSBs remain undetermined. Furthermore, while, in other material systems, the impact of an electrical field on an isolated metal inclusion in a solid-state ionic conductor is well-documented,[26] similar observations are lacking for Li metal and Li-ion conducting solids.[6]

In this study, we aim to directly observe a Li-metal inclusion that is electronically isolated and ionically connected (i-Li) in $Li_7La_3Zr_2O_{12}$ (LLZO) under an external electrical field. For this purpose, we assemble symmetrical Li|LLZO|Li cells with a single-crystal electrolyte and demonstrate that (1) the i-Li metal within the solid electrolyte responds to an applied electrical field (i.e., field-driven migration), (2) mass redistribution of a polarized i-Li in a crack network generates further crack expansion, and (3) redeposition of metal Li in a depleted crack starts at the tip.

Our results have wide-ranging implications for solid-state batteries with Li-metal anodes and, to the best of our knowledge, demonstrate, for the first time, the field-driven migration of Li metal inside a single-crystal solid electrolyte. We demonstrate that this field-driven migration of i-Li can have severe consequences for the mechanical integrity of the electrolyte.

The initiation and propagation of cracks filled with Li metal ("dendrites") in solid-state electrolytes are influenced by factors such as externally applied load,[10,13] porosity and grain size,[27,28] applied current density,[13] temperature,[29] dopant content,[9,28] and asperities at the Li-metal electrolyte interface.[27,30] To remove some of these complexities, we use a fully optically transparent single-crystal LLZO in a symmetrical Li|LLZO|Li cell under galvanostatic conditions and constant uniaxial load, ranging between 0.23−1.5 mA/cm^2 and 2−4.7 MPa, respectively, for each experimental step (Figure 1, Table S1). We use LLZO due to its interface stability against Li metal and, thus, exclude the formation of an interphase.[5,6] We

Received: January 10, 2025
Revised: February 12, 2025
Accepted: March 13, 2025
Published: April 2, 2025

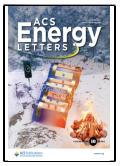

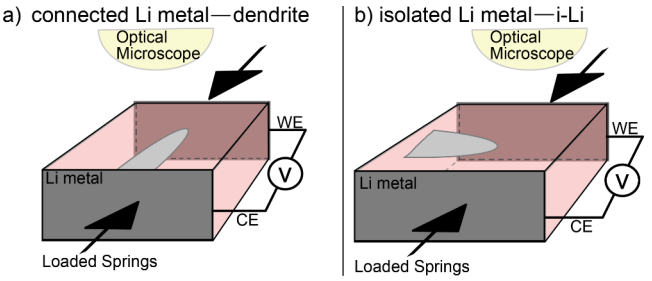

Figure 1. Schematic depicting the experimental setup used in this study. (a) Part one of this study reports results in a symmetrical Li|single-crystal LLZO|Li cell under an uniaxial load and constant current. (b) Part 2 of this study reports results in a symmetrical cell using the electrolyte from Part 1 reassembled with the electrodes rotated by 90°. This strategy generates a Li-filled crack that is electronically isolated and ionically connected (i-Li).

engineer an electronically isolated Li-metal inclusion (i-Li) by growing a dendrite similar to Figure 1a, and subsequently use the same electrolyte sample reassembled with electrodes rotated by 90° in a new cell, similar to Figure 1b (Table S1). For one experiment, we modify the setup in Figure 1 by adding a Whatman separator with liquid electrolyte (1 M $LiPF_6$ in PC) between the metal electrodes and the LLZO (see Figure S7). The addition of a separator prevents the growth of new dendrites and ensures that the lithium dendrite (i-Li) is fully electronically isolated. For details on sample preparation and electrode cleaning, see the Supporting Information.

LI DENDRITE PROPAGATION IN A SINGLE-CRYSTAL LLZO

Figures 2, S1, and S8 present *operando* observations of a dendrite growing in a single crystal at an applied nominal current density of j_n = 0.47 mA/cm^2 and an uniaxial load of 4 MPa (setup in Figure 1a, Table S1). The dendrites in Figure 2 have a planar, leaflike morphology and propagate at a rate of 8.6 μm/s (right dendrite) and 4.5 μm/s (left dendrite), respectively. Upon cell disassembly and electrode cleanup, we observe that the two dendrites are connected at the base and fully encapsulated in the LLZO crystal (Figures S3a, S6c, and S10). Our observations of dendrite morphology (Figures S3 and S6) resemble those of Yildirim et al.[8] and Reisecker et al.[31] in a similar single-crystal LLZO. We suggest that in a single-crystal LLZO the dendrites propagate as almost-2D objects (thickness of <2 μm, Figure S4) on the cleavage plane of the crystal.

After dendrite initiation, the local current density increases significantly compared with the nominally applied current density. The observed growth rate of the dendrites, dx/dt, in Figures 2 and S1 is enabled by a Li^+ flux concentration at the crack tip under a current density j_{tip}. We write the current, I, as $I = \frac{zF\,dV}{V_m^{Li}\,dt}$, where z = +1 for Li, F = 96485.3 C/mol is the Faraday constant, dV is the change in plated volume, and V_m^{Li} = 13.148 cm^3/mol is the molar volume of Li. Thus, the current density at the tip of the dendrite, j_{tip}, is expressed as

$$j_{tip} = \frac{I}{A} = \frac{zFA\,dx}{V_m^{Li}\,dt}\frac{1}{A} = \frac{zF}{V_m^{Li}}\frac{dx}{dt} \quad (1)$$

where the area at the tip of the dendrite (A) cancels out.[31] Note that eq 1 directly relates the observed growth rate to the current density at the crack tip, j_{tip}, independent of the nominally applied current density, j_n, or the number of simultaneously growing dendrites (Figures 2, S1). eq 1 presents an estimate of the current density at the extreme tip of the dendrite and excludes lateral growth (Figure S8). The growth rates observed in the experiment in Figure 2 correspond to values of j_{tip} = 6.3 A/cm^2 for the faster growing dendrite on the right of the image, and j_{tip} = 3.3 A/cm^2 for the dendrite on the left. These values are approximately 4 orders of magnitude larger compared to the nominal current density (j_n = 0.47 mA/cm^2), and highlight the strong localization enabled by Li-metal electrodeposition inside a narrow crack.

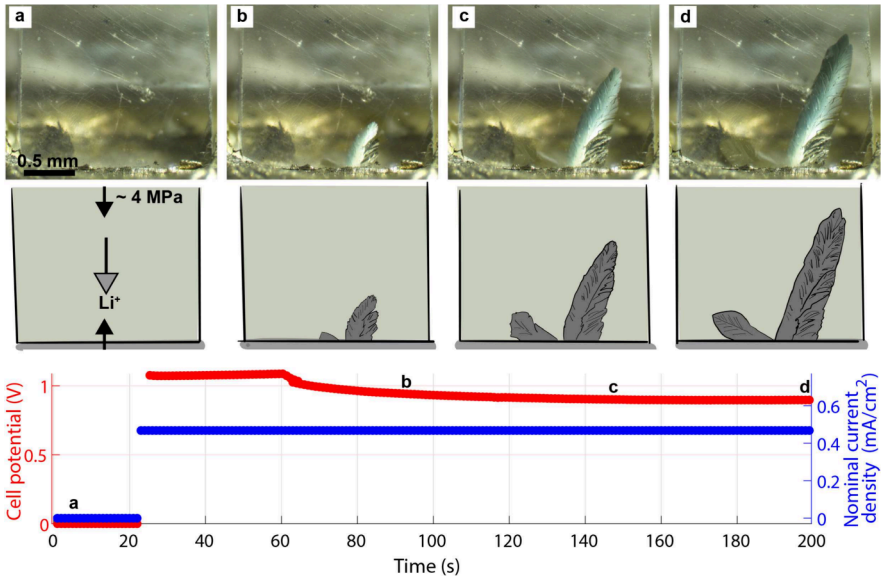

Figure 2. Key frames and corresponding illustrations of dendrite growth, alongside cell polarization and nominal current density, using a single-crystal LLZO in the experimental configuration presented in panel (a) (details in Table S1). The Li|LLZO interface in Figure 1a has residual asperities from sample preparation and polishing (see Figure S6), which enable dendrite initiation and growth in panels (b), (c), and (d).

https://doi.org/10.1021/acsenergylett.5c00101
ACS Energy Lett. 2025, 10, 2061−2067

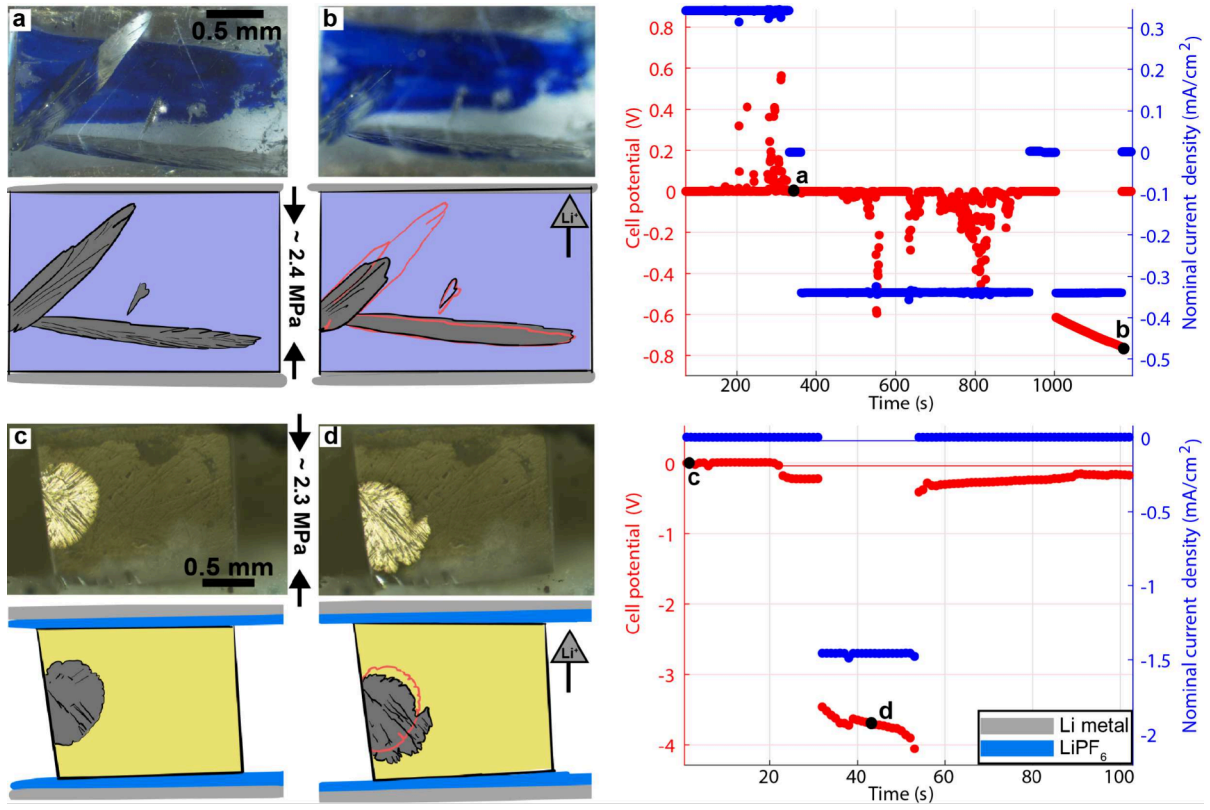

Figure 3. Selected key frames and corresponding schematic displaying evidence of field-driven migration of the bipolar i-Li in LLZO. Note that in panel (a), the Li-metal within the dendrite mirrors the blue marker dye on the bottom of the crystal. The experimental setup is depicted in Figures 1b and S7. Panels (a) and (b) correspond to a Li|LLZO|Li symmetrical cell, whereas panels (c) and (d) correspond to a cell containing two separators resulting in a Li|$LiPF_6$|LLZO|$LiPF_6$|Li cell. Further details can be found in Figures S2, S9, and Table S1.

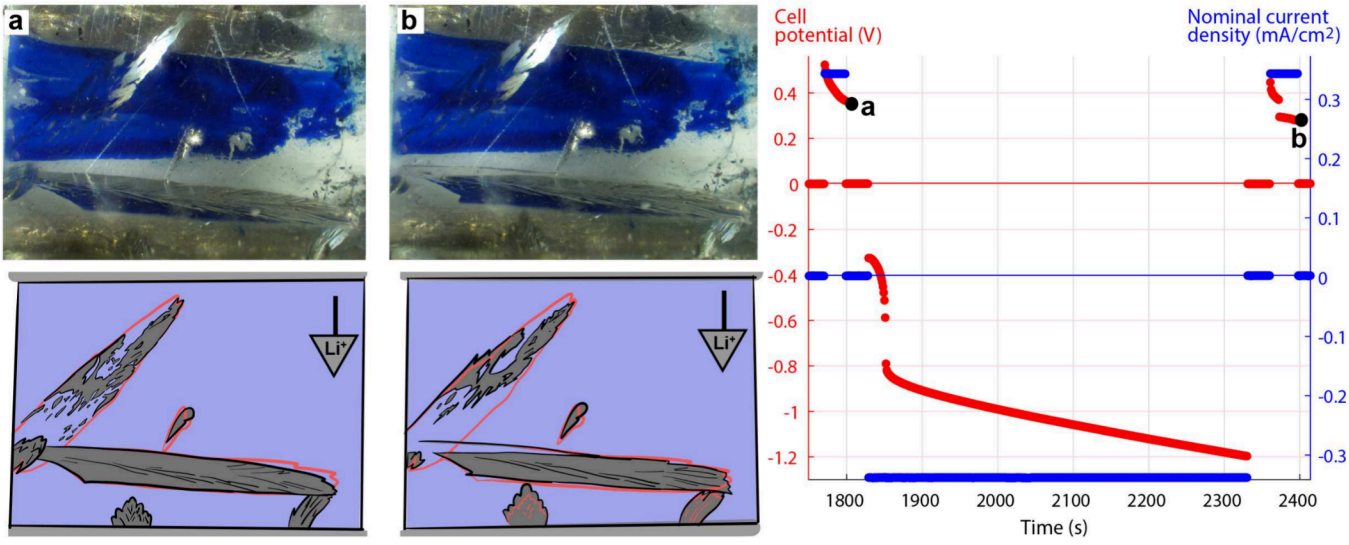

Figure 4. Selected key frames and corresponding schematic displaying evidence of inhomogeneous Li-metal replating in depleted cracks, starting at the tip of the crack. The experimental setup resembles Figure 1b. Further details can be found in Figure S2 and Table S1.

Our symmetrical cell setup has by design a near-zero open-circuit potential. Thus, the measured cell voltage, under galvanostatic conditions, represents the combined input of (1) ohmic resistance of the electrolyte (increases cell voltage, Figure 2), (2) dendrite nucleation at the plating electrode, followed by (3) dendrite propagation and decrease in effective electrode spacing (decreases cell voltage), (4) pore formation at the stripping electrode (increases cell voltage), and (5) charge-transfer resistance at interfaces (increasing cell voltage). Although we cannot deconvolute the contribution of the aforementioned processes, we suggest that the actual required overpotential for dendrite growth (item 3 above), ΔE_d, is a small fraction of the observed cell voltage in Figures 2 and S1. The maximum stress due to electrodeposition, $\sigma_{0,max}$, scales with the overpotential, according to $\sigma_{0,max} \approx -\frac{F}{V_m^{Li}}\Delta E_d$.[27] This

https://doi.org/10.1021/acsenergylett.5c00101
ACS Energy Lett. 2025, 10, 2061−2067

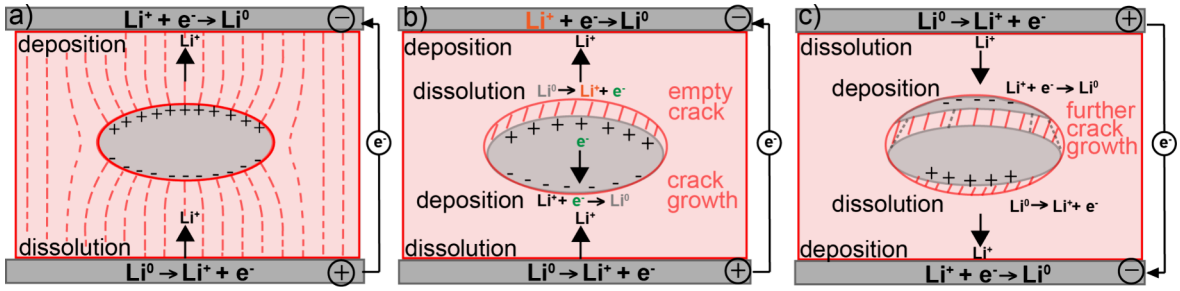

Figure 5. (a) Illustration of an electronically isolated (i-Li) inclusion in a solid electrolyte that becomes bipolar under an external electrical field. The presence of i-Li alters the field lines and enables two transport pathways. (b) The resulting charge separation due to polarization leads to simultaneous dissolution and deposition at the particle interfaces, generating the appearance of motion toward the positive electrode and an empty crack toward the negative electrode. (c) The reversal of the polarity of the external field leads to inhomogeneous redeposition toward the positive electrode. The dotted gray lines within the empty crack symbolize an electronic connection between the metallic inclusions that must be either present or form during replating into the empty crack.The black arrows correspond to the direction of the current in the LLZO and the metal inclusion.

stress ($\sigma_{0,max}$) is larger, compared to the stress required for crack propagation (σ), which is approximated as $\sigma \approx \frac{K_{IC}}{\sqrt{\pi a}}$, where a is the size of the initial surface flaw, and K_{IC} is the fracture toughness of LLZO (K_{IC} = 0.6 MPa $m^{1/2}$, measured on a similar single crystal by Swamy et al.[32]).[27] Thus, electrodeposition in defects on the length scale of a = 1 − 10 μm on the Li|LLZO interface (see Figures S1, S4, S6, S10), generates the required stresses for crack propagation ($\sigma \approx 0.33 - 0.1$ GPa) at relatively small overpotentials, $\Delta E_d \approx 40 - 13$ mV.[27]

The Impact of an Electrical Field on a Li-Metal Inclusion in LLZO. Our results demonstrate the field-driven migration of a Li-metal inclusion, which becomes a bipolar electrode[26] in LLZO under an electrical field. This phenomenon has been documented in a silver (Ag) particle on the surface of a silver bromide (AgBr) crystal,[26] and within a Li-metal island in a liquid electrolyte.[11] Figure 3 summarizes the impact of an electrical field on i-Li, using the setup presented in Figure 1b and S7b (see Figures S1 and S8 for the initial dendrite propagation). In Figures 3a and 3b, the isolated Li metal displays a shift in mass within the two interconnected cracks, which leads to further crack expansion in Figure 3b (the lower crack grows). Figures 3c and 3b present the field-driven migration of i-Li in a modified cell containing a separator with liquid electrolyte, resulting in a Li|$LiPF_6$|LLZO|$LiPF_6$|Li cell (see Figure S7). Similar to the all-solid-state cells, the i-Li shift generates further crack propagation. After the reversal of current direction, the Li metal redeposition starts at the tip and edges of the depleted crack network, as displayed in Figure 4 (detailed results using optical microscopy are given in Figures S2, S5, and S9 and corresponding supplementary videos outlined in Table S1). In later cycles, new dendrites connect the i-Li to the metal electrodes (Figures S2 and S5), except in the cell with a separator.

Figure 5 summarizes the mechanisms underpinning our observations (Figures 3, S5). In Figure 5a, the electrical field present within an i-Li inclusion in an LLZO matrix is altered by the redistribution of mobile electrons within the metal. Consequently, the i-Li develops negatively (LLZO|Li(−)) and positively (Li(+)|LLZO) charged regions at the interfaces with the adjacent LLZO[11,33] (Figure 5a). The presence of the i-Li in the electrolyte enables two Li-ion transport pathways: (1) through the pristine LLZO, and (2) through the combined path of the inclusion and the LLZO. Charge transport through the pristine single-crystal LLZO (pathway 1) relies on ion hopping mechanisms in the electrolyte.[5] Transport via the polarized i-Li (pathway 2) entails a composite pathway through the solid electrolyte and two charge transfer steps at the inclusion-electrolyte interfaces (Figure 5a). The Li^+ ions convert into metal at the LLZO|Li(−) interface (deposition), while simultaneously Li metal dissolution at the Li(+)|LLZO interface enables the charge neutrality of the metal inclusion. These simultaneous phenomena generate a shift in the center of mass (i.e., appearance of motion) of the i-Li toward the positive electrode of the cell as displayed in Figure 5b. Unlike a liquid Li-ion conductor,[11] the LLZO does not flow to accommodate the Li deposition at the positively polarized end (LLZO|Li(+)) of the inclusion, and the resulting stresses lead to crack expansion in the neighboring LLZO (Figure 5b). Thus, the polarization of i-Li generates further crack propagation while the i-Li mass is conserved (Figures S2, S5).

The characteristics of a polarized i-Li inclusion impact the Li-ion transfer pathways within the cell and consequently, the overall cell impedance.[33] The shape, aspect ratio, and orientation of the i-Li inclusion with respect to the electrodes affect the electrical field inside the cell and, therefore, impact the relative contribution of each transport pathway and the impedance of the cell. In general, for a bipolar metal, there is an infinitesimally small energy threshold for the i-Li mass shift, in addition to the resistance to charge transfer at both interfaces of the inclusion and electrolyte. In the case of an infinitesimally small i-Li, the inclusion carries only small currents compared to the bulk electrolyte, which by definition requires that one Li atom is deposited and one is dissolved at the inclusion−electrolyte interface. For a bipolar metal inclusion within a solid, the relationship between cell overpotential and the length of the i-Li is directly impacted by the additional energy required for further crack propagation—an effect that is absent in liquid-only cells. The scaling between the i-Li length and the overpotential at the inclusion−electrolyte interface is documented in liquid cells by Liu et al.[11] Thus, while all i-Li inclusions become polarized, certain geometries (e.g., penny-shaped and oriented parallel to the electric field) can be particularly detrimental for the mechanical integrity of SBBs.

We observe Li replating into previously Li-filled cracks that are both electronically isolated (depleted i-Li regions, Figure 3c), and directly connected to one of the electrodes (depleted dendrites, Figures 4b and S5g). In our optical microscopy

https://doi.org/10.1021/acsenergylett.5c00101
ACS Energy Lett. 2025, 10, 2061−2067

observations, the replating starts in patches at the crack tip or edges, where the distance from the positive electrode is minimal, and the replated Li metal has an inhomogeneous morphology (Figures 4 and S5). This observation requires the existence of an electronic conductive pathway toward an apparently empty crack tip (Figure 5c). We suggest three possible, mutually compatible, transport paths through: (1) a residual, optically undetectable, Li-metal layer due to incomplete dissolution, (2) the LLZO fracture surface due the local changes in stoichiometry, and (3) the instantaneous deposition of trace amounts of Li metal on the crack surface generated during current reversal. The first transport path is the least likely, as it implies that the electrochemical force driving Li dissolution does not overcome the adhesion between the thin Li and LLZO, which has been documented as an interface with weak adhesion due to the relatively poor Li wetting of surfaces.[34−36] The second possible electron transport path relies on local changes in the electronic conductivity of the LLZO fractured surface (i.e., the density of states around the Fermi level). Moreover, local heterogeneities on the fracture surface of the LLZO can lead to increases in the local conductivity. The third possible electron transport path relies on the fast redeposition of an optically undetectable Li-metal layer on the crack surface, which enables preferential Li redeposition such that the electrode distance is reduced (i.e., at the crack tip). The Li patches we observe during redeposition in Figures 4 and S5 could be a consequence of Li dewetting at high homologous temperatures (0.66 for Li at room temperature) in order to minimize surface energy.[37] Each patch polarizes as an individual i-Li, and thus, contributes to the inhomogeneous lithium morphology at the crack tip. Morphological instability during the deposition of isolated metal toward the positive electrode has also been observed on the surface of AgBr, which has a lower estimated electronic conductivity of $\sim 10^{-9}$ S/cm (refs 26 and 38) when compared to LLZO with an electronic conductivity of $\sim 10^{-7}$–10^{-8} S/cm.[20] Furthermore, our observations highlight that the rate of redeposition in a Li-metal-depleted crack is faster compared to simultaneous crack opening and Li-metal plating during dendrite growth (Figure 2).

IMPLICATIONS FOR SOLID-STATE BATTERIES

Our results have direct implications for all SSBs with metal anodes, which could contain metallic inclusions in the electrolyte due to heterogeneous plating and stripping or cell assembly. Solid-state cells rely on ceramic electrolytes manufactured through various techniques (e.g., tape casting,[39,40] pulsed laser deposition,[41] powder aerosol deposition[42]) leading to large variability in porosity, electrolyte thickness, and grain-size distribution. This microstructural heterogeneity can lead to asymmetric Li plating and stripping and eventual "dead" Li formation.[13−15] Within the same electrolyte sample, differences in grain-boundary electrical and mechanical properties enable heterogeneous ionic and electronic conductivities leading to Li-metal deposition in subsurface voids[25,43] and at susceptible grain boundaries,[19,21,44] which can become subsequently polarized and accelerate electrolyte damage. Particles of i-Li can also form as a consequence of battery architecture, such as engineered 3D electrolytes acting as a porous frame for Li plating[40] or multilayered structures.[45] Thus, cycling SSBs with i-Li generates further crack opening or new cracks with each cycle and accelerates mechanical damage.

In summary, we have demonstrated that Li-metal inclusions in a solid-state electrolyte exhibit bipolarity and field-driven migration. Our strategy of removing and rotating the electrodes in a symmetrical cell with a single-crystal electrolyte after dendrite growth creates an electronically isolated and ionically connected inclusion (i-Li). The current through the cell generates an electrical field around the i-Li (leading to polarization), which provides the driving force for further crack expansion due to simultaneous deposition and dissolution of Li metal under high hydrostatic stresses within the crack. We expect this mechanism to operate in solid-state batteries with alkali metal anodes that have "dead" metal inclusions and suggest that the polarization of these particles in SSBs is particularly destructive due to their ability to accelerate mechanical damage within the cell.

ASSOCIATED CONTENT

Supporting Information

The Supporting Information is available free of charge at https://pubs.acs.org/doi/10.1021/acsenergylett.5c00101.

Extended experimental methods, details of galvanostatic experiments, and *operando* results (PDF)
(ZIP)

AUTHOR INFORMATION

Corresponding Authors

Diana Avadanii − *Institute for Applied Materials IAM, Karlsruhe Institute of Technology KIT, 76131 Karlsruhe, Germany*; orcid.org/0000-0003-4534-1485; Email: diana.avadanii@kit.edu

Reiner Mönig − *Institute for Applied Materials IAM, Karlsruhe Institute of Technology KIT, 76131 Karlsruhe, Germany*; orcid.org/0000-0003-1048-9973; Email: reiner.moenig@kit.edu

Authors

Steffen Ganschow − *Leibniz-Institut für Kristallzüchtung IKZ, 12489 Berlin, Germany*; orcid.org/0000-0003-1328-1617

Markus Stypa − *Leibniz-Institut für Kristallzüchtung IKZ, 12489 Berlin, Germany*

Sonja Müller − *Institute for Applied Materials IAM, Karlsruhe Institute of Technology KIT, 76131 Karlsruhe, Germany*

Sabrina Lang − *Institute for Applied Materials IAM, Karlsruhe Institute of Technology KIT, 76131 Karlsruhe, Germany*

Dominik Kramer − *Institute for Applied Materials IAM, Karlsruhe Institute of Technology KIT, 76131 Karlsruhe, Germany*

Christoph Kirchlechner − *Institute for Applied Materials IAM, Karlsruhe Institute of Technology KIT, 76131 Karlsruhe, Germany*

Complete contact information is available at: https://pubs.acs.org/10.1021/acsenergylett.5c00101

Notes

The authors declare no competing financial interest.

ACKNOWLEDGMENTS

The authors thank Mr. Edmund Böck for technical support in manufacturing the optical cell setup. D.A. thanks Dr. Xufei Fang for stimulating conversations.

REFERENCES

(1) Albertus, P.; et al. Challenges for and pathways toward Li-metal-based all-solid-state batteries. *ACS Energy Lett.* **2021**, *6*, 1399−1404.
(2) Schmaltz, T.; Hartmann, F.; Wicke, T.; Weymann, L.; Neef, C.; Janek, J. A Roadmap for Solid-State Batteries. *Adv. Energy Mater.* **2023**, *13*, 2301886.
(3) Kazyak, E.; García-Méndez, R. Recent progress and challenges for manufacturing and operating solid-state batteries for electric vehicles. *MRS Bull.* **2024**, *49*, 717−729.
(4) Janek, J.; Zeier, W. G. Challenges in speeding up solid-state battery development. *Nat. Energy* **2023**, *8*, 230−240.
(5) Samson, A. J.; Hofstetter, K.; Bag, S.; Thangadurai, V. A bird's-eye view of Li-stuffed garnet-type Li 7 La 3 Zr 2 O 12 ceramic electrolytes for advanced all-solid-state Li batteries. *Energy Environ. Sci.* **2019**, *12*, 2957−2975.
(6) Krauskopf, T.; Richter, F. H.; Zeier, W. G.; Janek, J. Physicochemical concepts of the lithium metal anode in solid-state batteries. *Chem. Rev.* **2020**, *120*, 7745−7794.
(7) Ning, Z.; Li, G.; Melvin, D. L.; Chen, Y.; Bu, J.; Spencer-Jolly, D.; Liu, J.; Hu, B.; Gao, X.; Perera, J.; et al. Dendrite initiation and propagation in lithium metal solid-state batteries. *Nature* **2023**, *618*, 287−293.
(8) Yildirim, C.; Flatscher, F.; Ganschow, S.; Lassnig, A.; Gammer, C.; Todt, J.; Keckes, J.; Rettenwander, D. Understanding the origin of lithium dendrite branching in Li6.5La3Zr1.5Ta0.5O12 solid-state electrolyte via microscopy measurements. *Nat. Commun.* **2024**, *15*, 8207.
(9) Flatscher, F.; Todt, J.; Burghammer, M.; Søreide, H.-S.; Porz, L.; Li, Y.; Wenner, S.; Bobal, V.; Ganschow, S.; Sartory, B.; et al. Deflecting dendrites by introducing compressive stress in Li7La3Zr2O12 using ion implantation. *Small* **2024**, *20*, 2307515.
(10) Fincher, C. D.; Athanasiou, C. E.; Gilgenbach, C.; Wang, M.; Sheldon, B. W.; Carter, W. C.; Chiang, Y.-M. Controlling dendrite propagation in solid-state batteries with engineered stress. *Joule* **2022**, *6*, 2794−2809.
(11) Liu, F.; Xu, R.; Wu, Y.; Boyle, D. T.; Yang, A.; Xu, J.; Zhu, Y.; Ye, Y.; Yu, Z.; Zhang, Z.; et al. Dynamic spatial progression of isolated lithium during battery operations. *Nature* **2021**, *600*, 659−663.
(12) Chen, X.-R.; Yan, C.; Ding, J.-F.; Peng, H.-J.; Zhang, Q. New insights into "dead lithium" during stripping in lithium metal batteries. *J. Energy Chem.* **2021**, *62*, 289−294.
(13) Kazyak, E.; Garcia-Mendez, R.; LePage, W. S.; Sharafi, A.; Davis, A. L.; Sanchez, A. J.; Chen, K.-H.; Haslam, C.; Sakamoto, J.; Dasgupta, N. P. Li penetration in ceramic solid electrolytes: operando microscopy analysis of morphology, propagation, and reversibility. *Matter* **2020**, *2*, 1025−1048.
(14) Sun, H.; Liu, Q.; Chen, J.; Li, Y.; Ye, H.; Zhao, J.; Geng, L.; Dai, Q.; Yang, T.; Li, H.; et al. In situ visualization of lithium penetration through solid electrolyte and dead lithium dynamics in solid-state lithium metal batteries. *ACS Nano* **2021**, *15*, 19070−19079.
(15) Hu, X.; Zhang, Z.; Zhang, X.; Wang, Y.; Yang, X.; Wang, X.; Fayena-Greenstein, M.; Yehezkel, H. A.; Langford, S.; Zhou, D.; et al. others External-pressure−electrochemistry coupling in solid-state lithium metal batteries. *Nat. Rev. Mater.* **2024**, *9*, 305−320.
(16) Cao, T.; Xu, R.; Cheng, X.; Wang, M.; Sun, T.; Lu, J.; Liu, X.; Zhang, Y.; Zhang, Z. Chemomechanical Origins of the Dynamic Evolution of Isolated Li Filaments in Inorganic Solid-State Electrolytes. *Nano Lett.* **2024**, *24*, 1843−1850.
(17) Fang, C.; Li, J.; Zhang, M.; Zhang, Y.; Yang, F.; Lee, J. Z.; Lee, M.-H.; Alvarado, J.; Schroeder, M. A.; Yang, Y.; et al. Quantifying inactive lithium in lithium metal batteries. *Nature* **2019**, *572*, 511−515.
(18) Guo, W.; Shen, F.; Liu, J.; Zhang, Q.; Guo, H.; Yin, Y.; Gao, J.; Sun, Z.; Han, X.; Hu, Y. In-situ optical observation of Li growth in garnet-type solid state electrolyte. *Energy Storage Mater.* **2021**, *41*, 791−797.
(19) Song, Y.; Yang, L.; Zhao, W.; Wang, Z.; Zhao, Y.; Wang, Z.; Zhao, Q.; Liu, H.; Pan, F. Revealing the short-circuiting mechanism of garnet-based solid-state electrolyte. *Adv. Energy Mater.* **2019**, *9*, 1900671.
(20) Han, F.; Westover, A. S.; Yue, J.; Fan, X.; Wang, F.; Chi, M.; Leonard, D. N.; Dudney, N. J.; Wang, H.; Wang, C. High electronic conductivity as the origin of lithium dendrite formation within solid electrolytes. *Nat. Energy* **2019**, *4*, 187−196.
(21) Aguesse, F.; Manalastas, W.; Buannic, L.; Lopez del Amo, J. M.; Singh, G.; Llordés, A.; Kilner, J. Investigating the dendritic growth during full cell cycling of garnet electrolyte in direct contact with Li metal. *ACS Appl. Mater. Interfaces* **2017**, *9*, 3808−3816.
(22) Sun, M.; Liu, T.; Yuan, Y.; Ling, M.; Xu, N.; Liu, Y.; Yan, L.; Li, H.; Liu, C.; Lu, Y.; et al. others Visualizing lithium dendrite formation within solid-state electrolytes. *ACS Energy Lett.* **2021**, *6*, 451−458.
(23) Tian, H.-K.; Liu, Z.; Ji, Y.; Chen, L.-Q.; Qi, Y. Interfacial electronic properties dictate Li dendrite growth in solid electrolytes. *Chem. Mater.* **2019**, *31*, 7351−7359.
(24) Tian, H.-K.; Xu, B.; Qi, Y. Computational study of lithium nucleation tendency in Li7La3Zr2O12 (LLZO) and rational design of interlayer materials to prevent lithium dendrites. *J. Power Sources* **2018**, *392*, 79−86.
(25) Zhao, J.; et al. In situ observation of Li deposition-induced cracking in garnet solid electrolytes. *Energy Environ. Mater.* **2022**, *5*, 524−532.
(26) Peppler, K.; Reitz, C.; Janek, J. Field-driven migration of bipolar metal particles on solid electrolytes. *Appl. Phys. Lett.* **2008**, *93*, 074104.
(27) Porz, L.; Swamy, T.; Sheldon, B. W.; Rettenwander, D.; Frömling, T.; Thaman, H. L.; Berendts, S.; Uecker, R.; Carter, W. C.; Chiang, Y.-M. Mechanism of lithium metal penetration through inorganic solid electrolytes. *Adv. Energy Mater.* **2017**, *7*, 1701003.
(28) Huang, X.; Lu, Y.; Guo, H.; Song, Z.; Xiu, T.; Badding, M. E.; Wen, Z. None-mother-powder method to prepare dense Li-garnet solid electrolytes with high critical current density. *ACS Appl. Energy Mater.* **2018**, *1*, 5355−5365.
(29) Wang, M.; Wolfenstine, J. B.; Sakamoto, J. Temperature dependent flux balance of the Li/Li7La3Zr2O12 interface. *Electrochim. Acta* **2019**, *296*, 842−847.
(30) Lee, K.; Sakamoto, J. Li Stripping Behavior of Anode-Free Solid-State Batteries Under Intermittent-Current Discharge Conditions. *Adv. Energy Mater.* **2024**, *14*, 2303571.
(31) Reisecker, V.; Flatscher, F.; Porz, L.; Fincher, C.; Todt, J.; Hanghofer, I.; Hennige, V.; Linares-Moreau, M.; Falcaro, P.; Ganschow, S.; et al. Effect of pulse-current-based protocols on the lithium dendrite formation and evolution in all-solid-state batteries. *Nat. Commun.* **2023**, *14*, 2432.
(32) Swamy, T.; Park, R.; Sheldon, B. W.; Rettenwander, D.; Porz, L.; Berendts, S.; Uecker, R.; Carter, W. C.; Chiang, Y.-M. Lithium metal penetration induced by electrodeposition through solid electrolytes: example in single-crystal Li6La3ZrTaO12 garnet. *J. Electrochem. Soc.* **2018**, *165*, A3648−A3655.
(33) Squires, T. M.; Bazant, M. Z. Induced-charge electro-osmosis. *J. Fluid Mech.* **1999**, *509*, 217−252.
(34) Wang, J.; Wang, H.; Xie, J.; Yang, A.; Pei, A.; Wu, C.-L.; Shi, F.; Liu, Y.; Lin, D.; Gong, Y.; Cui, Y. Fundamental study on the wetting property of liquid lithium. *Energy Storage Mater.* **2018**, *14*, 345−350.
(35) Wang, M.; Sakamoto, J. Correlating the interface resistance and surface adhesion of the Li metal-solid electrolyte interface. *J. Power Sources* **2018**, *377*, 7−11.
(36) Han, X.; Gong, Y.; Fu, K.; He, X.; Hitz, G. T.; Dai, J.; Pearse, A.; Liu, B.; Wang, H.; Rubloff, G. Negating interfacial impedance in garnet-based solid-state Li metal batteries. *Nat. Mater.* **2017**, *16*, 572−579.
(37) Thompson, C. V. Solid-State Dewetting of Thin Films. *Annu. Rev. Mater. Res.* **2012**, *42*, 399−434.
(38) Zhao, J.; Buck, R. P. Influence of Contact Materials on Electric Properties of Single Crystal AgBr. *J. Electrochem. Soc.* **1989**, *136*, 3342.
(39) Fu, Z.; Zhang, L.; Gritton, J. E.; Godbey, G.; Hamann, T.; Gong, Y.; McOwen, D.; Wachsman, E. Probing the mechanical

https://doi.org/10.1021/acsenergylett.5c00101
ACS Energy Lett. 2025, 10, 2061−2067

properties of a doped Li7La3Zr2O12 garnet thin electrolyte for solid-state batteries. *ACS Appl. Mater. Interfaces* **2020**, *12*, 24693−24700.
(40) Yang, C.; Zhang, L.; Liu, B.; Xu, S.; Hamann, T.; McOwen, D.; Dai, J.; Luo, W.; Gong, Y.; Wachsman, E. D.; Hu, L. Continuous plating/stripping behavior of solid-state lithium metal anode in a 3D ion-conductive framework. *Proc. Natl. Acad. Sci. U. S. A.* **2018**, *115*, 3770−3775.
(41) Pfenninger, R.; Struzik, M.; Garbayo, I.; Stilp, E.; Rupp, J. L. A low ride on processing temperature for fast lithium conduction in garnet solid-state battery films. *Nat. Energy* **2019**, *4*, 475−483.
(42) Nazarenus, T.; Sun, Y.; Exner, J.; Kita, J.; Moos, R. Powder Aerosol Deposition as a Method to Produce Garnet-Type Solid Ceramic Electrolytes: A Study on Electrochemical Film Properties and Industrial Applications. *Energy Technol.* **2021**, *9*, 2100211.
(43) Shen, F.; Dixit, M. B.; Xiao, X.; Hatzell, K. B. Effect of pore connectivity on Li dendrite propagation within LLZO electrolytes observed with synchrotron X-ray tomography. *ACS Energy Lett.* **2018**, *3*, 1056−1061.
(44) Raj, R.; Wolfenstine, J. Current limit diagrams for dendrite formation in solid-state electrolytes for Li-ion batteries. *J. Power Sources* **2017**, *343*, 119−126.
(45) Doerrer, C.; Metzler, M.; Matthews, G.; Bu, J.; Spencer-Jolly, D.; Bruce, P. G.; Pasta, M.; Grant, P. S. Spraying Li6PS5Cl and silver-carbon multilayers to facilitate large-scale fabrication of all-solid-state batteries. *Device* **2024**, *2*, 100468.

https://doi.org/10.1021/acsenergylett.5c00101
ACS Energy Lett. 2025, 10, 2061−2067